Provided for non-commercial research and education use.
Not for reproduction, distribution or commercial use.

(This is a sample cover image for this issue. The actual cover is not yet available at this time.)

This article appeared in a journal published by Elsevier. The attached copy is furnished to the author for internal non-commercial research and education use, including for instruction at the authors institution and sharing with colleagues.

Other uses, including reproduction and distribution, or selling or licensing copies, or posting to personal, institutional or third party websites are prohibited.

In most cases authors are permitted to post their version of the article (e.g. in Word or Tex form) to their personal website or institutional repository. Authors requiring further information regarding Elsevier's archiving and manuscript policies are encouraged to visit:

http://www.elsevier.com/copyright

Author's personal copy

Quaternary Science Reviews 65 (2013) 26–38

Contents lists available at SciVerse ScienceDirect

Quaternary Science Reviews

journal homepage: www.elsevier.com/locate/quascirev

Controls on interior West Antarctic Ice Sheet Elevations: inferences from geologic constraints and ice sheet modeling

Robert P. Ackert Jr. [a,*], Aaron E. Putnam [b,f], Sujoy Mukhopadhyay [a], David Pollard [c], Robert M. DeConto [d], Mark D. Kurz [e], Harold W. Borns Jr. [f]

[a] Department of Earth and Planetary Sciences, 20 Oxford St., Harvard University, Cambridge, MA 02138, USA
[b] Lamont-Doherty Earth Observatory, Comer 217, P.O. Box 1000, Palisades, NY 10904, USA
[c] Earth and Environmental Systems Institute, Pennsylvania State University, University Park, PA 16802, USA
[d] Department of Geosciences, University of Massachusetts, Amherst, MA 01003, USA
[e] Department of Marine Chemistry and Geochemistry, Woods Hole Oceanographic Institution, Woods Hole, MA 02543, USA
[f] Climate Change Institute, University of Maine, Orono, ME 04469, USA

ARTICLE INFO

Article history:
Received 15 September 2012
Received in revised form
27 December 2012
Accepted 30 December 2012
Available online

Keywords:
WAIS
^{3}He
^{36}Cl
^{40}Ar/^{39}Ar
Exposure dating
Ice sheet model
Mt. Waesche
Ohio Range

ABSTRACT

Knowledge of the West Antarctic Ice Sheet (WAIS) response to past sea level and climate forcing is necessary to predict its response to warmer temperatures in the future. The timing and extent of past interior WAIS elevation changes provides insight to WAIS behavior and constraints for ice sheet models. Constraints prior to the Last Glacial Maximum (LGM) however, are rare. Surface exposure ages of glacial erratics near the WAIS divide at Mt. Waesche in Marie Byrd Land, and at the Ohio Range in the Transantarctic Mountains, range from ~10 ka to >500 ka without a dependence on elevation. The probability distribution functions (PDF) of the exposure ages at both locations, are remarkably similar. During the last glaciation, maximum interior ice elevations as recorded by moraines and erratics were reached between 10 ka and 12 ka. However, most exposure ages are older than the LGM and cluster around ~40 ka and ~80 ka. The peak in the exposure age distributions at ~40 ka includes ages of alpine moraine boulders at Mercer Ridge in the Ohio Range. Comparison of the PDF of exposures ages from the Ohio Range and Mt. Waesche with the temperature record from the Fuji Dome ice core indicates that the youngest peak in the exposure age distributions corresponds to the abrupt warming during the Last Glacial termination. A prominent peak in the Ohio Range PDF corresponds to the penultimate termination (stage 5e). During the intervening glacial period, there is not a consistent relationship between the peaks in the PDF at each location and temperature. A combined ice sheet/ice shelf model with forcing scaled to marine $\delta^{18}O$ predicts that interior WAIS elevations near the ice divide have varied ~300 m over the Last Glacial cycle. Peaks in the PDF correspond to model highstands over the last 200 ka. In the simulated elevation history, maximum ice elevations at Ohio Range (+100 m) and Mt. Waesche (+60 m) occur at ~10 ka, in agreement with observations from these sites. During collapse of the marine portion of the WAIS, ice elevations at Ohio Range and Mt. Waesche are drawn down at least 200 m below the present ice elevation. The good correspondence between the model results and observations at both the Ohio Range and Mt. Waesche supports the conclusion that interior WAIS highstands do not occur during glacial maximums. Rather, the highstands are controlled primarily by increased accumulation during temperature maximums that occur early in the interglacials. Interior down-draw events follow highstands, resulting from the arrival of a wave of thinning triggered by retreat of the WAIS grounding line coupled with decreasing accumulation rates.

© 2013 Elsevier Ltd. All rights reserved.

1. Introduction

Over the last decade, new glacial geologic and ice core data combined with ice sheet models indicate that the WAIS did not approach equilibrium during the Last Glacial Maximum (LGM) (Ackert et al., 1999; Waddington et al., 2005; Ackert et al., 2007; Price et al., 2007). While changes at the peripheral, marine-based margins of the WAIS, have been driven primarily by ice sheet/ocean interactions, the interior of the ice sheet is thought to respond primarily to changes in accumulation rates controlled largely by temperature e.g. (Alley and Whillans, 1984; Steig et al.,

* Corresponding author. Tel.: +1 617 496 6449; fax: +1 617 496 6958.
E-mail address: rackert@fas.harvard.edu (R.P. Ackert).

0277-3791/$ – see front matter © 2013 Elsevier Ltd. All rights reserved.
http://dx.doi.org/10.1016/j.quascirev.2012.12.017

Author's personal copy

2001). Thus, during the LGM (~20 ka), when the WAIS was at its maximum extent in the Ross and Weddell Seas (Anderson et al., 2002), interior ice-surface elevations were no higher than present, and possibly lower. Maximum surface elevations in the interior occurred during the early Holocene at ~10 ka as a result of increased accumulation (a consequence of maximum atmospheric temperatures) over cold, slowly flowing ice formed during the glacial maximum, prior to the arrival of a wave of thinning that propagated inland following grounding line retreat (Ackert et al., 1999; Steig et al., 2001; Ackert et al., 2007; Ackert et al., 2011). However, WAIS behavior prior to the LGM remains poorly constrained. In this regard, surface exposure ages of erratics and bedrock on mountains projecting through the WAIS provide opportunities to gauge past ice sheet elevations over timescales ranging from thousands to millions of years (Ackert et al., 1999; Stone et al., 2003; Ackert et al., 2007; Mackintosh et al., 2007; Ackert et al., 2011).

We focus on two sites within interior West Antarctica: Mt. Waesche and the Ohio Range. Mt. Waesche (77° 13′S; 125° 5′W) is a volcano projecting through the WAIS near the dome in Marie Byrd Land (Fig. 1). At the opposite end of the WAIS divide, the Ohio Range (85°S; 114°W) forms an east-west trending escarpment rising 500 m above the adjacent surface of the WAIS in the Horlick Mountains (Fig. 1). Features common to both Mt. Waesche and the Ohio Range are local ablation (blue ice) areas that result from interaction of prevailing winds with topography. Moraines and erratics deposited along the ice margin in long-lived local ablation areas directly record past changes in interior ice sheet elevation within the accumulation area of the Antarctic ice sheet. However, significant amounts of exposure of boulders may occur on the blue ice surface prior to deposition on the adjacent ice-free terrain, complicating the interpretation of exposure age distributions. In the Ohio Range, clasts with exposure ages >200 ka occur on the WAIS surface (Ackert et al., 2011; Fogwill et al., 2012).

At Mt. Waesche, surface exposure ages of basalt erratics indicate that ice elevations stood at least ~45 m above the present level at ~10 ka (Ackert et al., 1999). A single exposure age indicates that ice elevations were possibly as much 85 m above the present ice elevation at ~12 ka. In the Ohio Range, granite erratics extend ~125 m above the present WAIS elevation. Exposure ages of 10.5 ka and 12.5 ka were obtained from erratics along the trim line (Ackert et al., 2007). However, at both sites, most of the sampled erratics have older exposure ages ranging from the LGM to >500 ka that have the potential to provide information on earlier WAIS history.

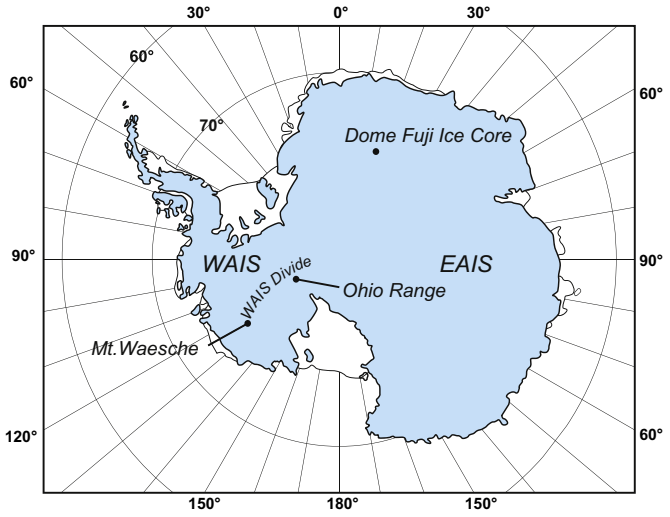

Fig. 1. Map of Antarctica showing the location of field sites and ice cores discussed in the text.

Outstanding questions regarding the pre-LGM WAIS history include: What is the timing and extent of earlier WAIS highstands and collapse events? What is the extent and duration of draw down of the land-based portions of the WAIS during collapse of the marine portions of the ice sheet? What is the response of the ice sheet in interior Antarctica to warmer temperatures? To address these questions, we report new ^{3}He and ^{36}Cl exposure ages of basalt erratics above the present WAIS surface at Mt. Waesche, and ^{3}He exposure ages of dolerite and sandstone boulders from ice-cored moraines of local alpine moraines in the Ohio Range. These data, along with ^{10}Be and ^{3}He exposure ages of granite erratics from the Ohio Range (Ackert et al., 2011) are compared to an ice core temperature record and WAIS elevation changes simulated by a continental ice sheet model. We conclude that in interior West Antarctica the peaks in exposure age distributions are linked to rising ice levels and relative highstands resulting from increased regional accumulation, as well as, locally higher ablation (sublimation) rates during periods of increased temperatures.

2. Geologic setting and methods

Descriptions of the geologic setting, sampling procedures, and analytical methods appear in earlier reports that highlighted the youngest exposure ages from the most recent WAIS highstands at Mt. Waesche and the Ohio Range Escarpment (Ackert et al., 1999; Ackert et al., 2007). In interior WAIS, extremely low subaerial erosion rates and non-erosive cold-based ice results in the pervasive occurrence of bedrock and regolith with long exposure to cosmic radiation (Mukhopadhyay et al., 2012). On the other hand, low erosion rates mean that for samples younger than ~125 ka, cosmogenic nuclide concentrations are not significantly affected by erosion. Thus, while erratics with prior exposure are expected, anomalously young exposure ages are unlikely; samples with the lowest apparent exposure ages (erosion rate = 0) provide the best estimate of the most recent highstand of the WAIS (Ackert et al., 2007; Mackintosh et al., 2007; Johnson et al., 2008; Stone et al., 2003; Bentley et al., 2010; Todd et al., 2010). However, most erratics at Mt. Waesche and the Ohio Range have apparent exposure ages older than the most recent highstand, but significantly younger than that of local bedrock outcrops (Ackert et al., 1999; Ackert et al., 2011; Mukhopadhyay et al., 2012), These samples are not readily distinguished by surface characteristics from those with the youngest exposure ages, and are not likely to have experienced significant erosion. A brief summary of the sampling locations and previous results from Mt. Waesche and the Ohio Range Escarpment appears below. In addition, we provide more detailed descriptions from the Ohio Range of the ice-cored lateral moraines of alpine glaciers bordering Mercer Ridge on Mt. Schopf.

2.1. The Ohio Range

2.1.1. Ohio Range Escarpment

The Ohio Range Escarpment exposes Permian sandstones and tillites overlying granitic basement rocks. Ablation zones (blue ice areas) occur on the western sides of Darling and Discovery Ridge in the lee of the prevailing winds as well as on the alpine glaciers (Fig. 2). Extensive areas of ice-cored moraine occur on the WAIS within the blue ice areas. We conducted transects from the WAIS ice margin to the peaks of several nunataks within the blue ice area west of Darling Ridge and on the escarpment at Darling and Discovery Ridge. In the Ohio Range, granite erratics lacking evidence of subaerial weathering are rare. Hence, we focused on clasts with

Author's personal copy

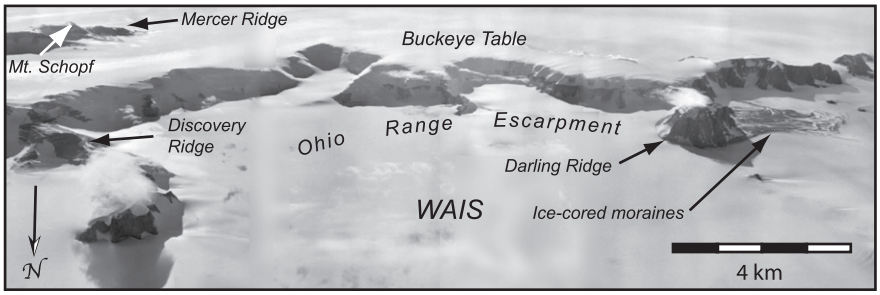

Fig. 2. Composite of oblique air photographs (TMA 575 R Frames 11, 12 and 13) looking toward the south, showing the WAIS, Ohio Range Escarpment and the locations discussed in the text.

sharp angular edges that differed in lithology from the local bedrock in order to differentiate erratics from locally derived rockfall. A trim line marking the last WAIS highstand was mapped from distribution of glacial deposits, erosional features, and the relative weathering of the underlying bedrock and dates to ~11 ka based on ^{10}Be exposure ages of the youngest erratics (Ackert et al., 2007).

On the Ohio Range Escarpment, the predominance of granite erratics makes quartz the preferred target mineral for cosmogenic nuclide measurements. At Antarctic temperatures, He diffusion rates in quartz are low enough that He is significantly retained for up to 100 ka (Brook and Kurz, 1993). ^{3}He was measured in 60 samples to screen for prior exposure; 43 of the samples were from erratics on bedrock and the rest were boulders from ice-cored moraines on the WAIS surface. ^{10}Be was measured in a subset of 15 samples encompassing the range of measured ^{3}He (Ackert et al., 2011) (Supplementary Tables 1 and 2). Based on an excellent correlation between the ^{3}He and ^{10}Be concentrations in the subset of samples, "equivalent ^{10}Be concentrations" were determined from the ^{3}He concentrations of the remaining samples using a quadratic equation which produced the best fit to the data ($R^2 = 0.99$). "Equivalent ^{10}Be exposure ages" were calculated from the equivalent ^{10}Be concentrations, propagating uncertainties in the ^{3}He measurements and curve fitting (Ackert et al., 2011). The resulting PDF of the exposure age distribution show peaks in probability at ~15 ka, ~75 ka, ~130 ka, and ~180 ka. The non-random distribution, with peaks corresponding to both the last and the penultimate glacial terminations, supports the validity of using the equivalent ^{10}Be exposure ages, at least for the granite lithologies in the Ohio Range. The peaks in the exposure age distribution correspond to pulses in the emergence of englacial debris in the blue ice areas related to warmer temperatures, increased snow accumulation and greater ice flux into the local ablation areas (Ackert et al., 2011).

2.1.2. Mercer Ridge

Above the escarpment is a broad ice-covered plateau, known as the Buckeye Table (Fig. 2). Two peaks rise above the plateau; the highest peak, Mt. Schopf, supports several alpine glaciers on its southern flank and is capped by a columnar jointed Ferrar Dolerite sill. Several alpine glaciers flow off the southern slopes of Mt. Schopf (Fig. 3a). Given their small, localized accumulation and ablation areas, these glaciers provide an independent record of changes in ice mass balance at the Ohio Range that can be compared with WAIS elevation changes along the ice divide. The lack of melting on these alpine glaciers (ablation is primarily through sublimation), suggests glacial expansions are likely due to increases in snow accumulation resulting from warmer temperatures rather than to decreased ablation due to cooler temperatures.

We retain the descriptive nomenclature of Mercer (1963) and refer to the alpine glaciers as North, Central and South Glaciers. North Glacier lacks moraines and glacial debris. Central Glacier flows westward into the Buckeye Table ice cap and thence into the EAIS, whereas the South Glacier flows southeasterly directly into the EAIS (Fig. 3a). Small ablation areas occur along the margins abutting Mercer Ridge. Two sets of lateral moraines are mapped along the southern margin of Central Glacier (Fig. 3b). The younger (proximal) set consists of three sub-parallel ice-cored ridges extending from a distinct moraine ridge at the drift edge down to a thin ice-cored moraine along the present glacier margin. The older (distal) lateral moraine consists of a relatively short segment that is cross-cut by the most distal of the younger ice-cored moraines. Only the younger set of ice-cored moraines occurs along the South Glacier. One of the most distal of the younger moraine ridges can be traced continuously over the top of the largely ice-free Mercer Ridge, indicating that the South Glacier and Central Glacier advanced synchronously (Fig. 3b).

In general, the sandstone and dolerite clasts comprising the younger moraine set are only slightly weathered. Rock weathering is limited to thin desert varnish and staining with weathering rinds less than 1 mm thick; essentially un-weathered clasts occur on the ice surface. However, even amongst the youngest moraines, some boulders have thick desert varnish or pits on one face, indicating prolonged exposure in outcrop. In contrast to the younger moraine set, there is pronounced weathering of all of the boulders comprising the older moraine. Dolerite boulders have rinds >1 mm, desert varnish and pits while the sandstone boulders exhibit cavernous weathering and deep staining.

Subglacial erosion is assumed to be negligible in these relatively thin, cold-based glaciers. Molded or striated clasts indicative of subglacial erosion were not observed. However, angular sandstone boulders and clasts are common on the moraines. Because sandstone does not presently crop out in the headwalls above the accumulation areas of the glaciers, we infer that the sandstone boulders were quarried subglacially. Although unweathered rockfall scars on the headwalls attest to recent rockfall events that may be large enough to contribute some dolerite debris with little inherited cosmogenic nuclides, this debris would constitute only a small component of rockfall. In order to limit the potential of prior exposure, only boulders with minimal and uniform desert varnish (surface oxidation) were sampled on the younger moraines. Ten ^{3}He exposure ages were obtained from pyroxene separates from dolerite boulders and four were obtained on quartz grains from sandstones. In order to provide some constraint on the potential amount of prior exposure on the headwall, one additional large dolerite boulder (OMR-81; Table 1) from a patch of ice-cored debris on Central Glacier was sampled. This boulder has well-developed weathering on one face and was sampled on both the weathered and the opposite unweathered face. Photographs of Mercer Ridge, the moraines and typical samples are included in the Supplementary Materials.

Author's personal copy

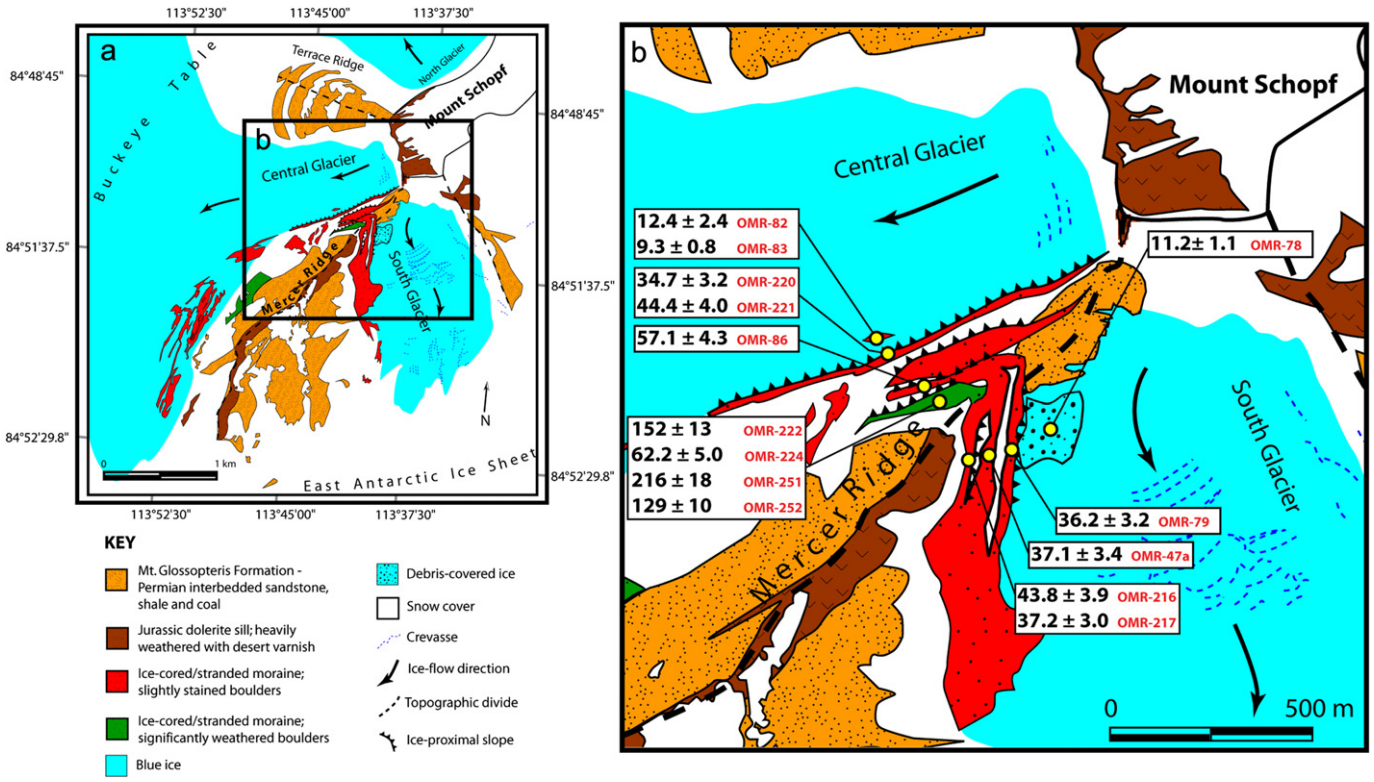

Fig. 3. a) Surficial geologic map of Mercer Ridge, South Glacier and Central Glacier on Mt. Schopf in the Ohio Range. b) Detail of the upper part of Mercer Ridge showing sample locations and exposure ages.

Table 1
Helium isotope data and exposure ages from alpine moraine boulders, Mt. Schopf.

Sample	Mineral	Elev.	Depth	Latitude	Longitude	^{4}He ± 1 sig	^{3}He/^{4}He ± 1 sig	^{3}He ± 1 sig	Age ± 1 sig
		m	cm	S	W	Atoms/g × 10^{13}	R/R_a	Atoms/g × 10^7	ka
Central Glacier									
Ice-cored debris patch on blue ice									
OMR-81a[a]	cpx	2210	2.5	84° 49.948′	113° 50.816′	37.7 ± 0.8	0.200 ± 0.003	9.90 ± 0.28	110 ± 9
OMR-81e	cpx	2210	2.0	84° 49.948′	113° 50.816′	41.7 ± 0.9	0.411 ± 0.006	23.2 ± 0.6	258 ± 22
OMR-82	cpx	2213	2.0	84° 49.944′	113° 50.694′	133 ± 5	0.026 ± 0.001	3.02 ± 0.27	12.4 ± 2.4
OMR-83	qtz	2213	3.0	84° 49.944′	113° 50.694′	5.78 ± 0.03	0.119 ± 0.003	0.95 ± 0.03	9.3 ± 0.8
1st moraine crest									
OMR-220	cpx	2206	4.0	84° 49.991′	113° 50.769′	41.3 ± 0.8	0.063 ± 0.002	3.04 ± 0.14	34.7 ± 3.2
OMR-221	cpx	2205	3.5	84° 49.990′	113° 50.827′	30.5 ± 0.6	0.102 ± 0.003	3.90 ± 0.16	44.4 ± 4.0
3d moraine crest									
OMR-86	qtz	2341	2.0	84° 50.061′	113° 48.576′	2.78 ± 0.01	2.16 ± 0.03	6.42 ± 0.08	57.1 ± 4.6
Older moraine crest									
OMR-222	cpx	2368	2.0	84° 50.088′	113° 48.762′	24.7 ± 0.5	0.443 ± 0.008	14.8 ± 0.4	152 ± 13
OMR-224	qtz	2368	2.0	84° 50.088′	113° 48.762′	4.92 ± 0.04	1.04 ± 0.01	7.02 ± 0.11	62.2 ± 5.0
OMR-251	cpx	2368	2.5	84° 50.084′	113° 48.611′	35.9 ± 0.7	0.444 ± 0.007	21.6 ± 0.5	216 ± 18
OMR-252	qtz	2368	2.0	84° 50.084′	113° 48.611′	2.10 ± 0.01	5.13 ± 0.05	14.9 ± 0.2	129 ± 10
South Glacier									
Boulder on blue ice									
OMR-78	cpx	2525	2.5	84° 50.156′	113° 44.365′	28.6 ± 0.5	0.041 ± 0.002	1.23 ± 0.08	11.2 ± 1.1
Inner ice-cored moraine									
OMR-79	cpx	2533	3.0	84° 50.248′	113° 45.102′	24.1 ± 0.5	0.131 ± 0.003	4.05 ± 0.14	36.2 ± 3.2
OMR-47a	cpx	2523	2.0	84° 50.276′	113° 45.621′	36.3 ± 0.7	0.093 ± 0.003	4.16 ± 0.17	37.1 ± 3.4
Outer ice-cored moraine									
OMR-216	cpx	2531	2.0	84° 50.326′	113° 45.696′	30.0 ± 0.5	0.129 ± 0.003	4.93 ± 0.17	43.8 ± 3.9
OMR-217	qtz	2527	2.0	84° 50.329′	113° 45.751′	2.64 ± 0.01	1.32 ± 0.02	4.79 ± 0.07	37.2 ± 3.0

cpx = clinopyroxene, qtz = quartz. R/R_a is the atmospheric ^{3}He/^{4}He = 1.384 × 10^{-6}. An initial ^{3}He/^{4}He of 0.010 ± 0.001 R/R_a is assumed for Dolerite samples (Ackert, 2000). All ^{3}He in quartz is assumed to be cosmogenic. The ^{3}He Production rates are 127 ± 10 atoms/g/yr for quartz and 111 ± 9 atoms/g/yr for pyroxene. The production rates were determined by normalizing the elemental production rates (Masarik and Reedy, 1996) to a production rate in olivine of 120 ± 9.8 atoms/g/yr (Goehring et al., 2010). Pyroxene compositions are from Ackert and Kurz (2004). Exposure ages are calculated assuming no erosion and include production rate uncertainties. Scaling is after Stone (2000). Furnace blanks for ^{3}He and ^{4}He were 7.8 × 10^3 and 8 × 10^8 atoms respectively. He isotopic ratios and concentrations were determined by normalizing to a standard with a ^{3}He/^{4}He = 8.8 R_a (HH3).

[a] Sample OMR-81 is a boulder with well-developed weathering on one side: samples a and e are from opposite sides and demonstrate prior exposure.

Author's personal copy

2.2. Mount Waesche

Mount Waesche (3200 m) is a volcano in the Executive Committee Range that projects through the WAIS south of the dome (~2000 m) in Marie Byrd Land (Fig. 1) and has been active during the Pleistocene (LeMasurier and Rex, 1989; LeMasurier and Kawachi, 1990). The southwestern flank is largely ice-free and moraines and drift composed of local volcanic debris extend up to 120 m above the ice surface (Ackert et al., 1999). Based on morphology, the moraines and drift are divided into an older upper band and a younger lower band. Both moraine bands consist of discontinuous ridges and hummocky drift; these features are more subdued on the upper moraine band. A few isolated drift patches also occur. These patches have subdued morphology but occur at lower elevation. An ice-cored moraine at the present WAIS margin has formed from tephra and pyroclastic layers that crop out in the blue ice exposed in the local ablation zone at the base of Mt. Waesche (Fig. 4). However, the basaltic glacial deposits comprising the upper and lower moraine bands lack a conspicuous pyroclastic component and thus may not have formed in an analogous manner. Weathering of the basalt clasts is limited to wind abrasion, fracturing and salt incrustations.

Samples of basalt boulders were collected for exposure dating from two transects across the moraine bands, from an isolated patch of ice-cored moraine near the WAIS margin and from supra-glacial debris on the ice sheet (Fig. 4). ^{3}He exposure ages were obtained from olivine and pyroxene bearing basalts; ^{36}Cl exposure ages were obtained from whole rock analyses of basalt samples lacking olivine or pyroxene (Ackert et al., 1999). ^{3}He exposure ages on the lower moraine band, up to 45 m above the present surface cluster tightly with a mean of 10.0 ± 0.6 ka. Paired ^{36}Cl and ^{3}He ages of two of the ~10 ka samples, are concordant and consistent with simple exposure histories (no periods of extended cover). Two ^{3}He exposure ages from the supra-glacial debris in the blue ice are <900 years indicating debris emerging from the ice at present has minimal prior exposure. In contrast, seven ^{3}He exposure ages from the upper moraine band ranged between 11.6 ka and 219 ka. Although the oldest ages are found at the highest elevation, the youngest exposure age also occurs at the same location, which suggests WAIS elevation as high as 85 m above the present in the early Holocene (Ackert et al., 1999). Here we report an additional eight ^{3}He exposure ages (Table 2) and six ^{36}Cl exposure ages (Table 3) from the upper moraine band and an isolated moraine patch near the ice margin. Furthermore, we report five ^{40}Ar/^{39}Ar ages on a subset of moraine boulders that provide maximum ages for the moraines and constrain the potential amount of prior exposure (Table 4).

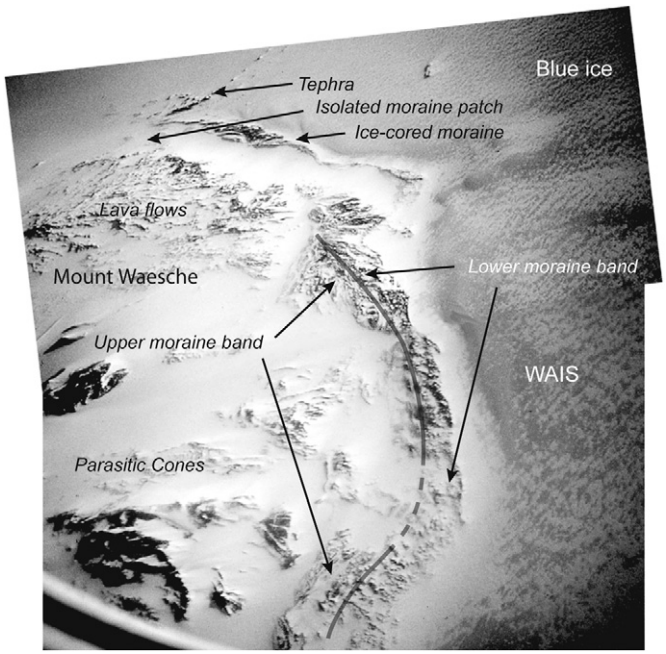

Fig. 4. Oblique aerial photograph of the southwestern flank of Mount Waesche and adjacent WAIS showing features mentioned in the text. The black line (dashed where inferred) separates the upper and lower moraine bands.

2.3. Exposure history of erratic boulders in the Antarctic interior

The interpretation of the pre-LGM exposure ages at Mt. Waesche and the Ohio Range Escarpment is not straightforward due to the lack of a clear relationship between exposure age and either elevation or location. As in other interior locations (Mackintosh et al., 2007; Lilly et al., 2010; Todd et al., 2010; Fogwill et al., 2012), a fundamental question is whether erratics with a range of prior exposure were deposited during a single highstand or whether the erratics were deposited with minimal prior exposure by cold-based ice during multiple highstands. Along the Ohio Range Escarpment, we interpret the cosmogenic nuclide concentrations in erratics as recording the total duration of exposure of the clasts in the ablation zone, including both initial exposure on the blue ice and subsequent exposure after deposition on adjacent ice-free terrain (Ackert et al., 2011). A similar conclusion was reached regarding the exposure history of erratics in the Heritage Range (Fogwill et al., 2012). We infer that the peaks in the exposure age distribution reflect pulses in supra-glacial debris accumulation in the blue ice areas. The pulses are linked to warmer temperatures, which would lead to higher ice fluxes due to increased regional accumulation rates and locally higher ablation rates in the blue ice areas. During the last WAIS highstand at ~11 ka, a portion of the supra-glacial debris with a range of exposure ages was deposited on the slopes and benches of the escarpment. While similar, earlier WAIS highstands and deposition of debris have likely occurred, they are not required to account for the observed distribution of exposure ages of erratics, as clasts with exposure ages >200 ka still occur on the ice-cored moraines on the WAIS surface (Ackert et al., 2011).

The depositional processes and exposure history of the erratics at Mt. Waesche likely differs in some respects from that in the Ohio Range. In contrast to the Ohio Range, the bedrock (lava flows) above the moraines at Mt. Waesche is relatively young (<500 ka: Table 4) and lacks the steep, deeply weathered surfaces with long exposure that would provide an unambiguous signature of prior exposure. A significant difference is that little supra-glacial debris occurs on the blue ice at Mt. Waesche at present. The very young exposure ages of clasts collected from the blue ice indicates that, as inferred in the Ohio Range, at least some material emerges in the ablation zone with minimal prior exposure (Ackert et al., 1999). Additionally, the two concordant ^{3}He and ^{36}Cl exposure ages of ~10 ka in basalt boulders from the lower moraine band is consistent with simple exposure histories without long periods of cover (Ackert et al., 1999).

Two models for the deposition and exposure history of the boulders sampled at Mt. Waesche with exposure ages >12 ka are considered. The first is that the boulders record episodes of WAIS thickening prior to the last highstand, with all or most exposure occurring after deposition of the boulders on the slopes of Mt. Waesche. Because a basalt boulder with a young exposure age (~12 ka) occurs on the upper moraine band, the model implies that the older samples were overridden during the last highstand and that multiple highstands have reached similar elevations. Alternatively, as in the Ohio Range, substantial exposure may occur on

Author's personal copy

Table 2
Helium isotopic data and exposure ages from Mt. Waesche, Marie Byrd Land.

Sample	Mineral	Elevation	Depth	Latitude	Longitude	^{4}He ± 1 sig	^{3}He/^{4}He ± 1 sig	^{3}He ± 1 sig	Age ± 1 sig
		m	cm	S	E	Atoms/g × 10^{10}	R/R_a	Atoms/g × 10^7	ka
WA-2-1	ol	1975	2.5	77° 13.89′	126° 55.07′	17.9 ± 0.2	470 ± 6.0	11.5 ± 0.2	141 ± 12
WA-2-2	**ol**	**1975**	3	**77° 13.89′**	**126° 55.07′**	**41.0 ± 0.3**	**316 ± 9**	17.6 ± 0.5	**219 ± 19**
WA-2-7	**ol**	**1975**	4	**77° 13.89′**	**126° 55.07′**	**14.8 ± 0.1**	**338 ± 9**	6.80 ± 0.20	**85.8 ± 7.7**
WA-2-10	**ol**	**1975**	3.5	**77° 13.89′**	**126° 55.07′**	**32.0 ± 0.3**	**155 ± 4**	6.60 ± 0.20	**82.9 ± 7.4**
WA-3A-1	ol	2035	2	77° 13.18′	127° 03.39′	12.1 ± 0.1	1217 ± 15	20.2 ± 0.3	237 ± 20
WA-3A-2	cpx	2035	2	77° 13.18′	127° 03.39′	9.17 ± 0.08	80.4 ± 1.8	0.95 ± 0.0	11.6 ± 1.0
WA-3A-3	**cpx**	**2035**	5	**77° 13.18′**	**127° 03.39′**	**7.19 ± 0.06**	**962 ± 27**	9.51 ± 0.28	**124 ± 11**
WA-3A-8	**ol**	**2025**	2	**77° 13.18′**	**127° 03.67′**	**7.53 ± 0.04**	**1715 ± 55**	17.8 ± 0.6	**210 ± 18**
WA-3B-1	ol	2025	2	77° 13.18′	127° 03.67′	6.00 ± 0.08	174 ± 6	1.39 ± 0.05	16.4 ± 1.5
WA-3B-2	ol	2025	3.5	77° 13.18′	127° 03.67′	14.7 ± 0.1	198 ± 3	3.90 ± 0.07	47.1 ± 4.0
WA-3B-5	**cpx**	**2025**	1	**77° 13.18′**	**127° 03.67′**	**12.7 ± 0.1**	**121 ± 4**	2.02 ± 0.07	**23.3 ± 2.0**
WA-4A-1	ol	2040	2	77° 12.13′	127° 06.29′	110.0 ± 1.1	40.9 ± 0.6	5.21 ± 0.11	60.8 ± 5.1
WA-4A-5	**cpx**	**2040**	1	**77° 12.13′**	**127° 06.29′**	**8.99 ± 0.02**	**570 ± 15**	7.01 ± 0.19	**84.5 ± 7.1**
WA-4B-1	ol	2035	2.5	77° 12.08′	127° 06.73′	52.2 ± 0.5	104 ± 3	7.07 ± 0.23	83.2 ± 7.3
WA-4B-3	ol	2035	2	77° 12.08′	127° 06.73′	2.50 ± 0.03	2201 ± 90	7.60 ± 0.32	88.7 ± 8.1
WA-4B-4	**cpx**	**2035**	2.5	**77° 12.08′**	**127° 06.73′**	**9.27 ± 0.02**	**487 ± 13**	6.17 ± 0.17	**76.5 ± 6.6**

New data in **Bold Type**. Other data are from Ackert et al. (1999). Ol = olivine; cpx = clinopyroxene. R/R_a is the atmospheric ^{3}He/^{4}He = 1.384 × 10^{-6}.
Mean magmatic ^{3}He/^{4}He is 6.6 ± 0.9 (R/R_a) n = 22. Exposure ages are calculated assuming no erosion and include production rate uncertainties. Scaling is after Stone (2000).
The same ^{3}He production rate is used for olivine and clinopyroxene (120 ± 9.8 atom/g/yr; Goehring et al., 2010).
Furnace blanks for ^{4}He ranged between 5 × 10^8 and 2 × 10^9 atoms. He isotopic ratios and concentrations were determined by normalizing to an air standard.

the blue ice prior to deposition on the slopes of Mt. Waesche, which is, however, in contrast to the present-day observations of minimal exposure in the blue ice areas (Section 2.2). During the last highstand, clasts with prior exposure ranging from near zero to ~200 ka were deposited on the flank of Mt. Waesche. As is the case in the Ohio Range, the latter model does not require multiple highstands, but is also compatible with some of the older exposure ages being deposited during earlier highstands.

2.4. Measurements of ^{3}He, ^{36}Cl and ^{40}Ar/^{39}Ar

The He measurements on Mt. Waesche basalts were carried out at the Woods Hole Oceanographic Institution following techniques outlined in (Kurz, 1986; Kurz et al., 1996). Olivine and pyroxene separates were crushed to determine the magmatic ^{3}He/^{4}He; the resulting powders were melted to determine the ^{3}He/^{4}He and ^{4}He concentration. Cosmogenic ^{3}He was determined by subtracting the magmatic ^{3}He from the total ^{3}He released by melting. The He measurements on dolerite and sandstone moraine boulders from Mercer Ridge were measured at the Noble Gas laboratory at Harvard University. After crushing and sieving, the 250–500 μm fraction was leached in either oxalic or hydrochloric acid for ~1 h. For the dolerite samples, the magnetic fraction was separated using a hand magnet and pyroxene, free of adhering plagioclase, was picked from the non-magnetic fraction using a binocular microscope. For sandstone, whole quartz grains free of visible inclusions were selected. The He isotopes were measured following analytical techniques outlined by Gayer et al. (2008).

Due to the lack of a significant magmatic component in the Ferrar Dolerite, the pyroxene samples were not crushed prior to melting in the furnace and all ^{4}He is assumed to be radiogenic (Ackert and Kurz, 2004). An inherited component with an ^{3}He/^{4}He of 0.010 ± 0.001 was assumed for dolerite based on measurements of shielded samples from the Dry Valleys (Ackert, 2000). Cosmogenic ^{3}He was determined by subtracting the inherited ^{3}He from the total ^{3}He. For quartz obtained from sandstones, all ^{3}He is assumed to be cosmogenic; we treat the ^{3}He exposure ages as minimum exposure ages due to helium loss from diffusion.

Chlorine-36 chemistry was performed in the cosmogenic nuclide laboratory at the University of Washington following procedures of Stone et al. (1996a) and Stone et al. (1996b) and ^{36}Cl measurements were made at PRIMElab. The ^{40}Ar/^{39}Ar analyses were made at the University of Wisconsin following procedures described in (Singer et al., 2004).

2.5. Description of the ice sheet model

We investigate the potential influence of ice sheet elevation changes on the exposure age distributions using a continental-scale ice sheet model that simulates Antarctic Ice Sheet dynamics over

Table 3
Chlorine data and exposure ages from Mt. Waesche, Marie Byrd Land.

Sample	Elevation	Latitude	Longitude	CaO	K_2O	$\sigma_{35}N_{35}/\Sigma$[a]	[Cl] ± 1 sig	Cl-36 ± 1 sig[b]	Age ± 1 sig[c]
	m	S	E	wt %	wt %		ppm	Atom/g × 10^5	ka
WA-3C-1	2000	77° 13.23′	127° 4.06′	5.17	2.36	0.00977	1145 ± 6	19.20 ± 0.66	91.1 ± 3.5
WA-3C-2	2000	77° 13.23′	127° 4.06′	5.12	2.31	0.00967	1185 ± 12	13.66 ± 0.56	65.0 ± 2.9
WA-3C-3	2000	77° 13.23′	127° 4.06′	4.99	2.44	0.00884	1227 ± 10	11.05 ± 0.48	42.0 ± 1.9
WA-3C-6	2000	77° 13.23′	127° 4.06′	5.16	2.37	0.00994	1175 ± 2	16.04 ± 0.63	76.1 ± 3.2
WA-3C-7	2000	77° 13.23′	127° 4.06′	5.02	2.75	0.00934	1270 ± 27	12.07 ± 0.66	47.0 ± 2.7
WA-4A-4	2040	77° 13.18′	127° 03.67′	10.63	0.86	0.00886	292 ± 1	14.54 ± 0.28	183.3 ± 4.4

[a] Fraction of thermal neutrons captured by ^{35}Cl.
[b] Corrections for radiogenic ^{36}Cl are <3.5%. ^{36}Cl decay constant 2.303 × 10^{-6}/yr. Procedural blank <3 × 10^5 atoms ^{36}Cl (^{36}Cl/Cl = 1.3 × 10^{-14}).
[c] Exposure ages calculated assuming no erosion and include production rate uncertainties. ^{36}Cl production rates at sea level and latitude >50°. P_{Ca} spallation = 48.8 ± 1.4 atoms/gCa/yr (Stone et al., 1996a). P_K spallation = 185 ± 15 atoms/gK/yr. (Stone et al., 1996b). P_{Ca} muon capture = 5.3 ± 1.0 atoms/gCa/yr (Stone et al., 1998). Neutron capture including thickness correction treated according to the method of Liu et al. (1994). Altitude scaling for spallation and muon reactions after Stone (2000).

Author's personal copy

Table 4
Summary of $^{40}Ar/^{39}Ar$ data from furnace incremental heating experiments.

Sample	Total fusion age (ka)	Age spectrum			Isochron analysis		
		Increments used (°C)	^{39}Ar (%)	Age ± 2 sig (ka)	*N*	$^{40}Ar/^{36}Ar$ ± 2 sig intercept	Age ± 2 sig (ka)
WA-2-2	339.6 ± 23.0	750–1190	83.3	328.8 ± 16.5	14 of 19	295.1 ± 3.8	334.5 ± 49.9
WA-3A-8	327.3 ± 38.7	715–1300	100.0	330.3 ± 31.0	12 of 12	293.2 ± 4.5	381.6 ± 99.2
WA-3A-3	278.9 ± 56.5	740–1260	100.0	255.1 ± 43.3	9 of 9	297.6 ± 3.2	198.4 ± 92.6
WA-3D-1	278.5 ± 28.0	840–1375	100.0	265.4 ± 16.2	10 of 10	296.7 ± 1.9	252.3 ± 26.3
WA-4C-1	556.0 ± 82.4	740–1300	100.0	558.4 ± 73.8	10 of 10	295.0 ± 2.6	585.0 ± 149.5

Ages calculated relative to 1.194 Ma Alder Creek Sandine at 1.194 Ma.
K decay constants: a) 0.581×10^{-10} yr^{-1}, b) 4.692×10^{-10} yr^{-1}.

the last 5 Ma (Pollard and DeConto, 2009). The simulated ice-elevation history since the early Pliocene is consistent with the geologic evidence and bedrock cosmogenic nuclide concentrations at the Ohio Range (Mukhopadhyay et al., 2012). The version used here (Pollard and DeConto, 2012a, 2012b) is similar to that presented in (Pollard and DeConto, 2009), but includes a new inversion scheme to deduce basal sliding coefficients and more physical parameterizations of ice shelf calving and sub-ice shelf melting. The model uses scaled dynamical equations for sheet and shelf flow depending on whether the ice is grounded or floating. Mass flux across the grounding line between the two domains is a function of ice thickness and incorporates the effects of ice shelf buttressing. Modern parameterizations of temperature and precipitation are scaled to marine $\delta^{18}O$ and the annual 80° S insolation anomaly. Sub-ice-shelf melting is parameterized based on the degree of protection by islands and bays and distance to the ice shelf edge. Sea level is scaled to marine $\delta^{18}O$ assuming the LGM corresponds to −125 m.

3. Results

3.1. Mercer Ridge

The He isotope data and ^{3}He exposure ages of dolerite and sandstone boulders from moraines of the Central and South Glacier on Mercer Ridge appear in Table 1. Both exposure ages (258 ka and 110 ka) from the boulder with well-developed weathering on one face (OMR-81) are significantly older than other samples from the younger moraines suggesting that prior exposure, when present, will be conspicuous. Most of the exposure ages ($n = 5$) cluster between 30 and 50 ka, with a peak centered at 35 ka (Fig. 5b). The samples that contribute to the 35 ka peak from South Glacier occur on all three sampled ice-cored moraine ridges. The exposure ages increase progressively from the moraine near the blue ice margin to the more distal moraines (Fig. 3b). On Central Glacier, samples contributing to the 35 ka peak also occur on the first ice-cored moraine outboard of the active ice margin, but the sample from the more distal moraine is older, ~57 ka (Fig. 3b).

There are also ^{3}He exposure ages of 12.4 ka and 9.3 ka from the ice-cored moraine on Central Glacier (dolerite) and of 11.2 ka from the blue ice of South Glacier (sandstone), which corresponds to the last WAIS highstand on the Ohio Range Escarpment (Fig. 5b; Table 1). Unlike the Ohio Range Escarpment, the exposure ages vary systematically, with older ages occurring on the more distal moraines. We take the clustering of these exposure ages, their systematic distribution and the occurrence of boulders with exposure ages of ~35 ka at multiple locations on two separate glaciers, as support for our assumption that the dolerite and sandstone boulders composing the lateral moraines are lacking significant prior exposure and were derived largely subglacially. This conclusion is also supported by the three exposure ages <12.4 ka obtained on samples collected on the blue ice.

The ^{3}He exposure ages of dolerite boulders (~152 ka and ~216 ka) from the older moraine predate the penultimate glaciation (isotope stage 6). The younger ^{3}He ages of the sandstone boulders from this moraine are treated as minimum ages both because of He diffusion and because the erosion rate of the friable lithologies is relatively high. Even so, the apparent exposure age of one sandstone boulder (~129 ka) predates the Last Interglacial. This moraine clearly records a much earlier expansion of the alpine glaciers.

3.2. Mount Waesche

^{3}He exposure ages ($n = 16$) from Mt. Waesche range between ~12 ka and 219 ka and appear in Table 2 and Fig. 5c. We do not include eight exposure ages from the lower moraine band as their interpretation is straightforward; they are tightly clustered and occur at a consistent elevation recording the position of the WAIS margin at ~10 ka (Ackert et al., 1999). Here we focus on samples from the upper moraine band ($n = 12$) and from an isolated patch of moraine near the present ice margin ($n = 4$) (Fig. 3). Six whole-rock ^{36}Cl exposure ages obtained on aphyric basalt from the upper moraine band range between 42 ka and 183 ka (Table 3). The PDF and histogram (Fig. 5c) incorporates both the ^{3}He and ^{36}Cl exposure ages <200 ka from the upper moraine band and the isolated moraine patch ($n = 21$). The exposure ages are clustered into three groups. Only three exposure ages are <23 ka, three exposure ages cluster around ~45 ka and ten fall within a broad cluster between 65 and 95 ka with a peak at ~85 ka ($n = 5$). The peak at ~10 ka would dominate if the exposure ages from the lower moraine band were included in the PDF. We conclude that as on the Ohio Range Escarpment, the exposure age distribution is not random and that the peaks in the exposure age distribution have geologic and/or glaciologic implications relating to past ice elevations at Mt. Waesche.

The $^{40}Ar/^{39}Ar$ ages of the basaltic moraine boulders range from ~200 to >500 ka and extend the known range of active volcanism on Mt. Waesche (Table 4). The $^{40}Ar/^{39}Ar$ ages indicate that the upper moraine band formed <255 ± 43 ka. The maximum amount of prior exposure varies by lithology ranging from ~250 ka to ~500 ka. The basalt boulder with the oldest eruption age has the youngest exposure age of ~10 ka. This result indicates that at least some basalt from very old lava flows is incorporated into the WAIS with little prior exposure suggesting that the basalt comprising the moraines is quarried subglacially.

3.3. Comparison of exposure age distributions from the Ohio Range and Mt. Waesche

We compare the exposure age distributions from Mercer Ridge (Fig. 5b) and Mt. Waesche (Fig. 5c) to the ^{3}He (equivalent ^{10}Be exposure ages) and ^{10}Be exposure ages of erratics and ice-cored moraine boulders from the Ohio Range Escarpment

Author's personal copy

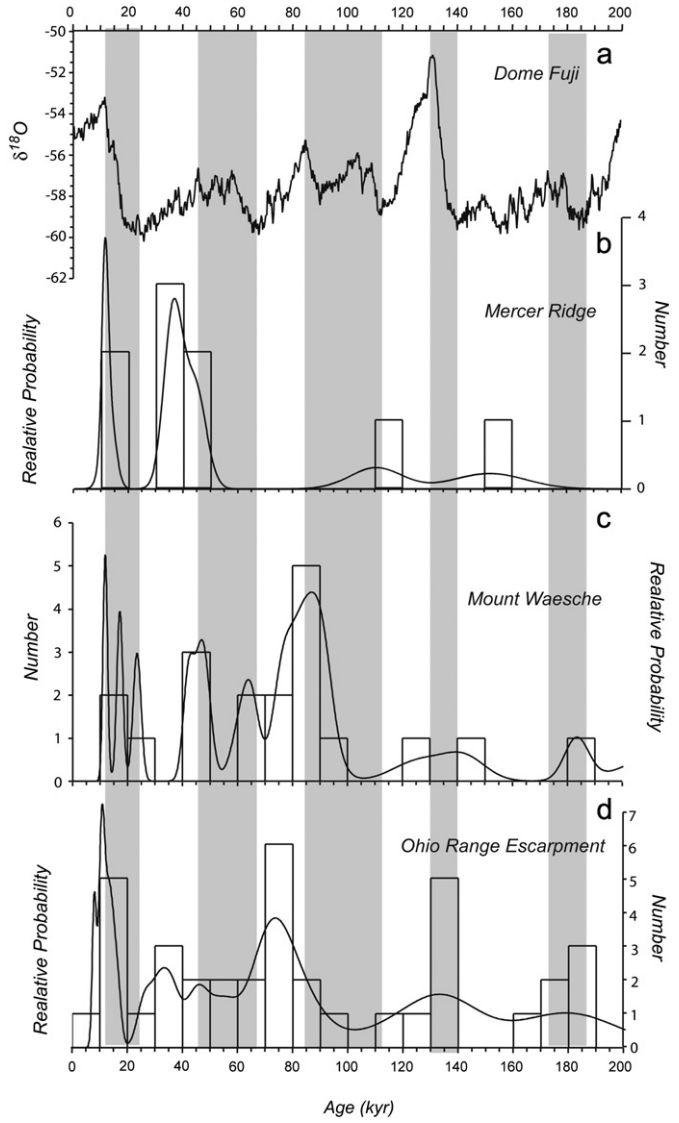

Fig. 5. a) The $\delta^{18}O$ record from the Fuji Dome Ice core in East Antarctica; $\delta^{18}O$ is a proxy for air temperature at the core site (Kawamura et al., 2007). The Fuji Dome Ice core record is similar to that from the Byrd Ice Core, which is located between Mt. Waesche and the Ohio Range in interior West Antarctica. The excellent agreement over their common range (10–90 ka) suggests that the Fuji Dome record is applicable to interior West Antarctica. b–d) Histograms and probability density functions (PDF) of exposure ages from interior West Antarctica. The exposure age distributions are truncated at 200 ka, as too few exposure ages >200 ka were measured to form meaningful distributions. b) ^{3}He exposure ages from dolerite boulders from ice-cored alpine moraines on Mt. Schopf. c) ^{3}He and ^{36}Cl exposure ages from basalt boulders from the upper moraine band and ice-cored moraine patch on Mt. Waesche. d) ^{10}Be exposure ages and equivalent ^{10}Be exposure ages calculated from ^{3}He concentrations from granite erratics on the Ohio Range Escarpment and the blue ice. Data are from Ackert et al. (2011). Tables with the ^{10}Be and ^{3}He data from Ackert et al. (2011) are in the Supplementary Materials. Gray bars indicate intervals of rising air temperature.

(Fig. 5d). The overall patterns of the exposure age distributions <100 ka at the Ohio Range and Mt. Waesche are remarkably similar, although the peak observed at 135 ka in the Ohio Range is absent at Mt. Waesche and Mercer Ridge. In all three locations, there is a peak corresponding to the last highstand at ~10 ka. However, the peaks in the exposure age distributions between 20 ka and 100 ka from the Ohio Range Escarpment and Mt. Waesche are offset. Peaks at 35 ka and 75 ka in the Ohio Range PDF correspond to peaks at 45 ka and 85 ka in the Mt. Waesche PDF. The dominant peak between 30 ka and 50 ka at Mercer Ridge overlaps both the younger peak at Mt. Waesche and the Ohio Range Escarpment.

Assuming the pattern of the exposure age distributions is meaningful, the offset in the peaks at the two locations could arise from a number of reasons. The offset may result from the choice of erosion rates and/or production rates used to calculate the exposure ages. Potential differences in erosion rates between Mercer Ridge (dolerite at >2200 m), the Ohio Range Escarpment (granite at ~1600 m elevation) and Mt. Waesche (basalt at ~2000 m elevation) are not accounted for. We have assumed an erosion rate of zero for all samples based on the lack of evidence of weathering on the samples and on very low long-term erosion rates (~20 cm/Ma) in the Ohio Range (Mukhopadhyay et al., 2012). Erosion rates an order of magnitude higher than those long term rates are required in order to shift the zero erosion rate ^{10}Be exposure ages from the Ohio Range by ~10 ka such that they align with the peaks in ^{3}He and ^{36}Cl exposure ages at Mt. Waesche. The evidence suggests this possibility is unlikely.

The offsets may reflect production rates uncertainties: ^{10}Be was utilized for granites and sandstone at the Ohio Range Escarpment, whereas ^{3}He and ^{36}Cl were utilized for basalts at Mt. Waesche and ^{3}He for dolerites at Mercer Ridge. We note that applying the recent Southern Hemisphere ^{10}Be production rate calibrations (Putnam et al., 2010; Kaplan et al., 2011) would bring the exposure age distributions into closer alignment. However, the prominent peak in the Ohio Range that now correlates with the penultimate termination (Fig. 5d; Ackert et al., 2011) would also become significantly older. Moreover, it remains unclear whether the lower ^{10}Be production rate is applicable in Antarctica or if the production rates of other cosmogenic nuclides need to be similarly reduced. For example, the new ^{10}Be production rate is too low to generate the steady-state ^{10}Be concentrations observed in old Antarctic bedrock surfaces (Nishiizumi et al., 1991; Ivy-Ochs et al., 1995; Balco and Shuster, 2009) and so cannot apply on million-year timescales without compensating changes in scaling factors. Thus, we doubt that production rate uncertainties alone are responsible for the observed offset.

Given the caveats above, the offset in the exposure age distributions between the last two glacial terminations from the Ohio Range Escarpment and Mt. Waesche may reflect actual differences in the exposure age distribution at the two sites. Both the response time of the WAIS to climate forcing during this interval, and the depositional processes at these locations may differ. However, the similarities in the PDF suggest the WAIS is responding to a common forcing.

3.4. Comparison of exposure age distributions with an ice core temperature record

The $\delta^{18}O$ of ice is a function of air temperature at the core site. We compare the exposure age distributions from our three field locations (Fig. 5b–d) with the $\delta^{18}O$ record from the Dome Fuji Ice core from East Antarctica (Fig. 5a), the nearest ice core with a record spanning the last 200 ka (Fig. 1) (Kawamura et al., 2007). This $\delta^{18}O$ record is very similar to that from the Byrd Ice Core, which lies between Mt. Waesche and the Ohio Range in West Antarctica but only extends back to ~90 ka (Johnsen et al., 1972). The similarity of the $\delta^{18}O$ records of the ice cores over their common range suggests that the Dome Fuji record is representative of climatic conditions across interior West Antarctica.

The $\delta^{18}O$ record from the Dome Fuji ice core is characterized by millennial-scale variability superimposed on strong Milankovitch-scale fluctuations, with a pattern similar to marine $\delta^{18}O$ records. Glacial terminations are characterized by large, abrupt increases in temperature (decreasing $\delta^{18}O$). The youngest peak in the PDF of

Author's personal copy

exposure ages from all three sites corresponds to the abrupt warming associated with the last termination. There is a significant peak in the histogram from the Ohio Range Escarpment that aligns with the warming at the penultimate termination (prior to stage 5e). This peak appears to be absent at the other locations. However, there are too few samples with ages >100 ka from either Mt. Waesche or Mercer Ridge to conclusively determine the presence or absence of older peaks at these sites. The lack of older exposure ages may simply reflect our sampling bias; sampling targeted boulders with little to no weathering as our focus was on constraining the last highstand. At Mt. Waesche the peaks at 45 ka and 85 ka correlate with intervals of peak warmth (Fig. 5c) whereas at Mercer Ridge (Fig. 5b) and the Ohio Range Escarpment (Fig. 5d) the corresponding peaks correlate with intervals of cooling. Thus, there does not appear to be a simple relationship between peaks in the exposure age distributions and temperature in interior West Antarctica other than during glacial terminations.

3.5. Ice elevation changes in interior WAIS as simulated by the ice sheet model

Large-scale results and time-series of the ice sheet model (Fig. 6) are essentially the same as in Pollard and DeConto (2009) and Ackert et al. (2011), but the simulated ice thickness over modern and LGM West Antarctica are notably improved. As a result, simulated absolute ice elevations at the Ohio Range and at Mt. Waesche are very close (±50 m) to actual observations (Figs. 7 and 8). In comparison, while the earlier version of the model utilized in Ackert et al. (2011) accurately predicted relative changes in ice elevation, absolute elevations were several hundred meters too high. Another difference between the model presented here and earlier versions (Ackert et al., 2011) is that down-draw of WAIS elevation at the Ohio Range during the Last Interglacial (stage 5), which was similar to the present in the earlier simulation, is now ~200 m lower due to more extensive collapse of the marine portions of the WAIS (Fig. 6a). The simulated draw down (Fig. 7), however, occurs at ~90 ka; i.e., draw down occurs after stage 5c rather than after stage 5e as observed in sea level records e.g. (Len Vacher and Hearty, 1989). Furthermore, collapse of the marine WAIS is still not as extensive as at other times in the simulation (Fig. 6c).

As in earlier versions of the model, the magnitude and relative frequency of WAIS collapse events is reasonable when compared to

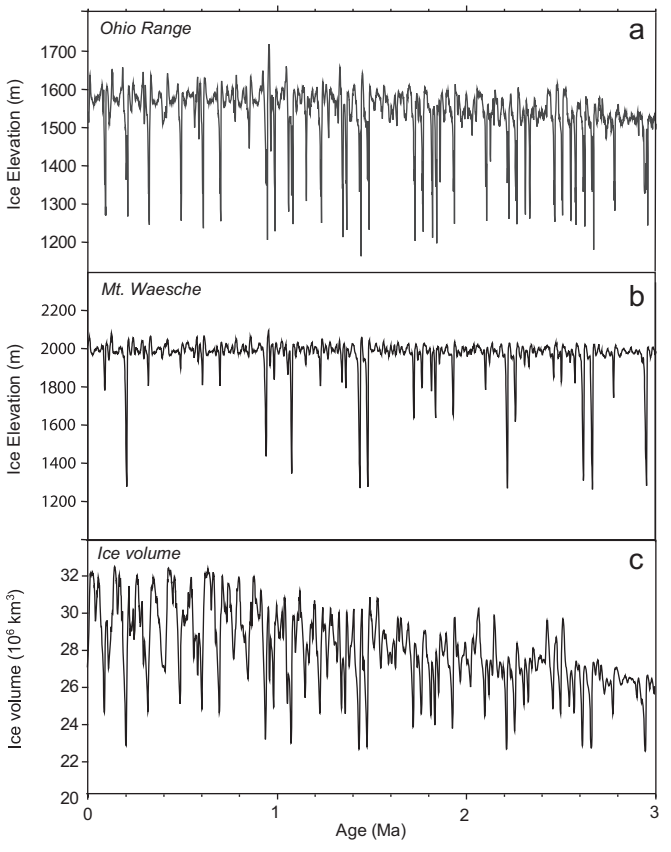

Fig. 6. Simulated WAIS elevation and volume changes from the ice sheet model over the last 3 Ma. The simulated elevation histories agree well with both the present day ice elevations and past elevation changes inferred at both the Ohio Range Escarpment and Mt. Waesche. Although the magnitude and frequency of full WAIS collapse events is reasonable, the timing of some specific collapse events may be erroneous. a) The simulated elevation history at the Ohio Range. Ice elevations have increased over the last 3 Ma. Down draw during most interglacials is ~200 m. b) The simulated elevation history at Mt. Waesche. Average ice elevations have remained relatively constant. Full WAIS collapse events with down draw of ~600 m are relatively rare. c) The simulated WAIS ice volume history. Maximum WAIS volume has increased significantly, while WAIS volume during collapse events has remained relatively constant. The Ohio Range elevation history and WAIS volume are from Ackert et al. (2011).

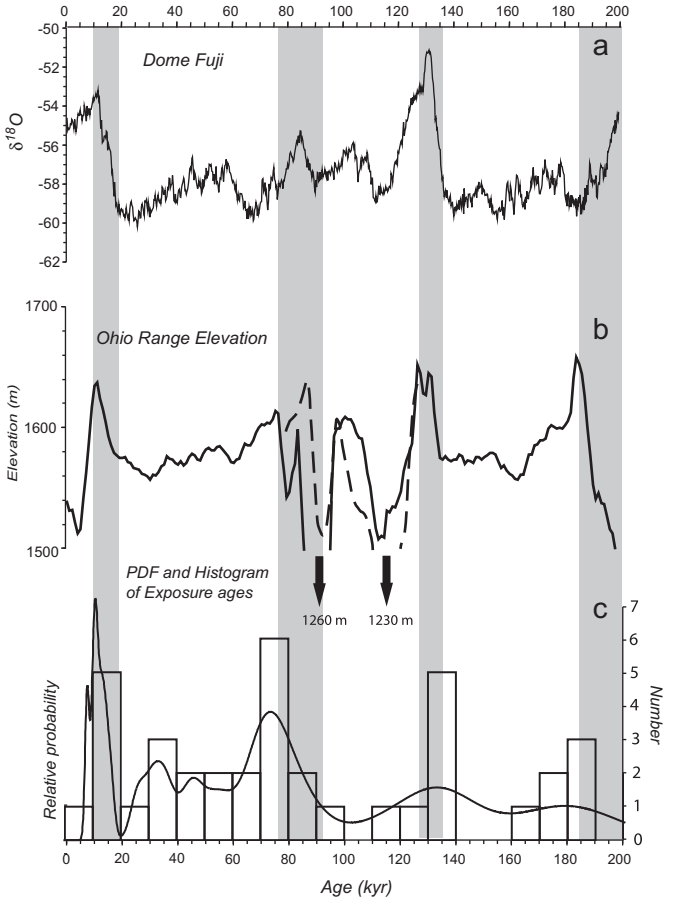

Fig. 7. a) The $\delta^{18}O$ record from the Dome Fuji Ice core in East Antarctica (see Fig. 5). b) Simulated WAIS elevation history at the Ohio Range from the ice sheet model (solid line) for the last 200 ka. The present ice elevation in the simulation is similar to that observed. In the simulation, WAIS collapse occurs at ~90 ka (stage 5c) rather than at 120 ka (stage 5e) as observed in relative sea level records. Dashed line is the previous collapse event in the simulation ~200 ka, transposed to stage 5e, which represents a more realistic scenario. The figure is truncated at 1500 m; arrows and elevations indicate the amount of simulated down draw during collapse events. c) Histogram and PDF of exposure ages from the Ohio Range. Peaks in the exposure age distribution correspond to intervals of rising ice elevation (gray bars).

Author's personal copy

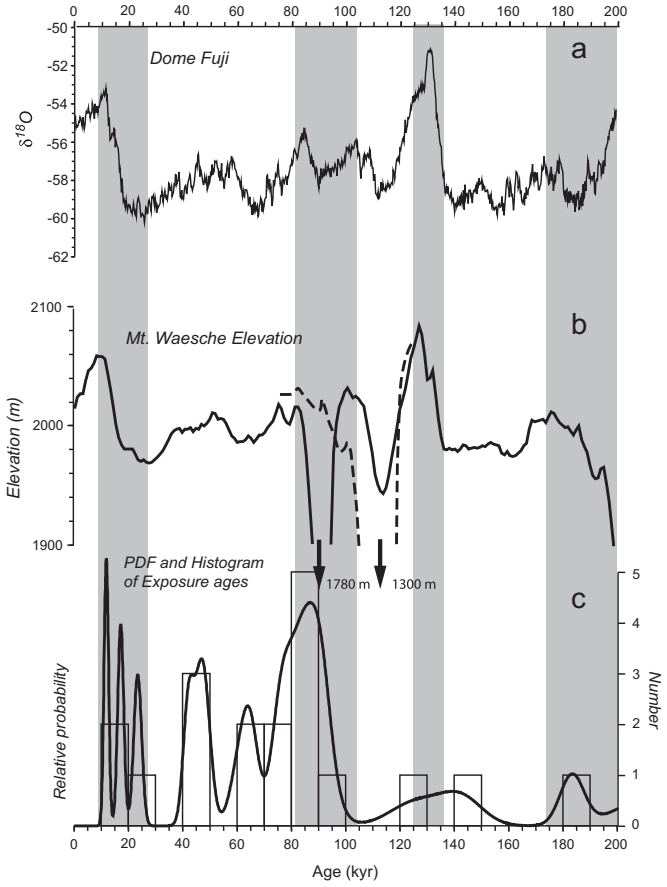

Fig. 8. a) The $\delta^{18}O$ record from the Dome Fuji Ice core in East Antarctica (see Fig. 5). b) Simulated WAIS elevation history at Mt. Waesche from the ice sheet model (solid line) for the last 200 ka. The present ice elevation in the simulation is similar to that observed. Similar to the Ohio Range, the elevation history is punctuated with brief WAIS highstands and down draw events associated with WAIS collapse, with the most recent WAIS collapse occurring ~90 ka (stage 5c) rather than at 120 ka (stage 5e). Dashed line and arrows as in Fig. 6. c) Histogram and PDF of exposure ages from Mt. Waesche. Peaks in the exposure age distribution correspond to intervals of rising ice elevation (gray bars).

global sea level records, but the timing of some specific Pleistocene collapse events may be erroneous (Fig. 6). We attribute this to the simple parameterization of sub-ice shelf melting that varies in proportion to the stacked benthic $\delta^{18}O$ record and a minor contribution of austral summer insolation, which is probably not a sufficiently accurate proxy for the timing and magnitude of incursions of warmer waters onto the Antarctic Shelf. We have tried other combinations of forcing, for instance involving the duration of austral summer (Huybers and Denton, 2008) or annual mean austral insolation, but we have not found a combination that yields substantially better timing of specific Pleistocene interglacial collapses.

However, once collapse of the WAIS is initiated, it is irreversible and progresses in a similar manner regardless of the details of background forcing. In the simulation, all full collapse events have a similar character, magnitude and duration (Fig. 6). Hence, for purpose of discussion, we have transposed an earlier, more extensive collapse event at ~200 ka in the simulation to stage 5e, when collapse of the marine portions of the WAIS likely occurred (dashed lines in Figs. 7 and 8) e.g. (Mercer, 1978;; Bamber et al., 2009). Assuming the model captures the physics, if not the timing of WAIS collapse, this composite curve represents a more probable ice elevation history at our sites.

4. Discussion

4.1. Chronology of alpine glacier expansion on Mercer Ridge

The history of expansion and retreat of alpine glaciers in interior Antarctica provides a test for ice sheet models that link snow accumulation rates to temperature. Summer temperatures in interior Antarctica remain well below freezing even during interglacial periods. Hence, ice ablation by melting is negligible, and changes in mass balance are thought to be dominated by changes in accumulation rates, which are positively correlated with temperature (Alley and Whillans, 1984). However, interior ice sheet thickness is also dependent on advected temperature changes at the base of the ice sheet that control ice velocity and the position of the ice sheet margins. Therefore, net changes in interior ice elevation are dependent on multiple factors. The mass balance of alpine glaciers is also predicted to increase during warmer intervals, but these glaciers are insensitive to changes in ice velocity in the ice sheet and fluctuations of the ice sheet margin that propagate into the interior. Thus, alpine glacier history potentially can be used to independently infer past changes in accumulation rates.

Interpreting exposure age distributions of these cold-based alpine glaciers is however, not as straightforward as their temperate counterparts. Because they are largely non-erosive, much of the englacial debris originates from rockfalls into the accumulation areas. Prior exposure of clasts is thus expected; only large or frequent rockfall events, or sub-glacial entrainment will introduce material with little prior exposure. As is the case for the surrounding Antarctic ice sheet, local ablation areas may be long-lived and accumulate supra-glacial debris where additional exposure may occur. Given these complications, the exposure age distribution of sampled dolerite moraine boulders from the alpine glaciers at Mercer Ridge is surprisingly tight with a peak centered on 35 ka ($n = 5$; Fig. 5b). This result suggests that we were largely successful in avoiding boulders with prior exposure in the headwall.

We consider two interpretations of the PDF at Mercer Ridge. The first is based on the common assumption that the exposure ages of moraine boulders date the end of moraine formation and the beginning of ice retreat. This interpretation implies that the advance of Central and South Glaciers peaked around 35 ka. Comparison of the exposure age distribution with the Fuji Dome $\delta^{18}O$ record (Fig. 5a) shows that formation of the ice-cored moraines at ~35 ka would correlate with cooling following the end of a 15 ka period of relative warmth in interior West Antarctica. Given our assumption that these alpine glaciers advance in response to increased accumulation (warmer temperatures), retreat during cooling temperatures is plausible. While this scenario links glacier advance and retreat to temperature driven accumulation changes, it begs the question of why the alpine glaciers are less extensive now during a period of much greater warmth than the period between 45 and 60 ka.

Alternatively, we consider an interpretation of the Mercer Ridge exposure age distribution that borrows from our interpretation of the exposure age distribution of erratics on the Ohio Range Escarpment, where most exposure of the boulders occurred after they emerged in the blue ice area, prior to deposition on the Escarpment during the last highstand at ~12 ka (Ackert et al., 2011). In this scenario, the ~35 ka peak in the Mercer Ridge PDF relates to a pulse in the accumulation of supra-glacial debris on the alpine glaciers. Relatively warmer temperatures between 45 and 60 ka (Fig. 5a) may have increased rockfall and/or subglacial quarrying. At present, rock surfaces are sometimes heated above 0 °C by solar insolation during the summer season introducing liquid water into fractures. Hence, because of the increased presence of liquid water in rock fractures during warm intervals, the rate of frost wedging and, consequently, rockfalls could increase.

Author's personal copy

Alternatively, the alpine glacier ice would be warmer and thicker during intervals of warmer atmospheric temperatures. The resulting increased ice velocities would favor increased subglacial quarrying.

Supraglacial debris would have likely accumulated in ice-cored bands as observed in other blue ice areas, such as that near Darling Ridge below the Escarpment (Fig. 2). Typically older bands are more distal, with the youngest, thinnest debris closest to the active ice margin. Maximum accumulation rates during the temperature maximum at ~10 ka could have resulted in advance of alpine glaciers synchronous with maximum WAIS elevations. We envision the supra-glacial debris bands riding the rising ice surface and remaining essentially intact. Subsequent thinning of the alpine glaciers since ~10 ka in response to cooling temperatures (Fig. 5a) resulted in the stranding of ice-cored supra glacial debris bands and the formation of ice-cored moraines. The youngest exposure ages from the blue ice proximal to the moraines would correspond to debris that emerged during the advance at ~10 ka.

Although the older (most distal) moraine crest at Mercer Ridge is a candidate for an alpine glacier expansion during the previous interglacial (Stage 5e), analogous to an advance at ~10 ka, all but one exposure age are older than 129 ka even assuming no erosion (Table 1). However, it is also more likely that these boulders have a ^{3}He component from exposure in the headwall prior incorporation into the moraine. While many samples with prior exposure can be avoided when sampling young moraines by exclusively sampling unweathered boulders, this strategy is not possible on older moraines where all boulders are weathered. Thus, while it remains possible that this moraine records alpine glacier expansion during the last or earlier interglacial periods, we do not correlate this moraine with a specific event in the Dome Fuji temperature record. Overall, the exposure age distribution on Mercer Ridge moraines are consistent with multiple interpretations that are consistent with glacial expansion due to increased accumulation rates during intervals of warmer temperature. Currently lacking information on the response of these cold-based glaciers to mass balance changes, differentiating between these scenarios is not possible. Additional work is required to fully understand the glacial and climatic history recorded by these unique glaciers from Mercer Ridge.

4.2. Comparison of exposure age distributions with elevation changes in the WAIS interior simulated by a continental ice sheet model

4.2.1. Elevation history of the WAIS at the Ohio Range Escarpment

As in the earlier version of the model (Ackert et al., 2011), the correlation of ice elevation at the Ohio Range Escarpment with the Dome Fuji ice core temperature record is readily apparent, with higher ice elevations corresponding to warmer temperatures (Fig. 7). Generally, model ice elevation in the Ohio Range is higher than present with highstands ~100 m above present occurring during maximum warmth following glacial terminations (Fig. 7). Consistent with observations that the most recent highstand is the highest level attained by the WAIS over the last 5 Ma (Mukhopadhyay et al., 2012), the height of WAIS highstands in the simulation in general increases over time (Fig. 6). However, cosmogenic nuclide concentrations in bedrock in the Ohio Range indicate that average ice elevations over the last 5 Ma have been at or below present elevations, indicating that the average ice elevation in the model is too high (Mukhopadhyay et al., 2012).

All of the prominent peaks in the exposure age distribution (Fig. 7c) correspond to rapidly rising and/or peaks in ice elevation. The correspondence of the prominent peak in exposure ages at 75 ka with the simulated rapid increase in ice elevation following the down-draw event is somewhat specious, as the timing of this collapse is likely incorrect. However, recovery from full WAIS collapse events earlier in the simulation (Fig. 6) typically takes two precession cycles (~40 ka) and it is therefore likely that the first relative ice sheet highstand after the Last Lnterglacial did occur around 80 ka (Fig. 7b; dashed line). Overall, the new simulation of WAIS elevation history at the Ohio Range matches the geologic observations well, in both the predicted timing and absolute elevation changes. Based on the model results, we suggest that the relative paucity of exposure ages between 90 ka and 130 ka is a result of draw down of the WAIS surface (~200 m) below the present elevation associated with collapse of the marine portions of the WAIS during the Last Interglacial (stage 5e). However, the existence of boulders from ice-cored moraines with exposure ages >130 ka on the WAIS surface suggests that ice-flow patterns along the Ohio Range Escarpment were not affected significantly and that down draw of areas grounded above sea level in this region of the WAIS, was limited (Ackert et al., 2011).

4.2.2. Elevation history of the WAIS at Mt. Waesche

The simulated elevation history for Mt. Waesche from the ice sheet model is shown in Figs. 6 and 8b. As in prior 2D models (Ackert et al., 1999), the last highstand occurs at ~10 ka, about 40 m above the present ice margin in good agreement with the exposure ages and absolute elevation of the lower moraine band. The simulated elevation changes at Mt. Waesche show a strong correlation with temperature changes inferred from the Fuji Dome ice core (Fig. 8). Highstands occur early in interglacial intervals due to high accumulation rates as in the Ohio Range. Down-draw events reflect collapse of the marine portions of the WAIS and propagation of a wave of thinning into the interior of the ice sheet combined with decreasing accumulation rates. In contrast, to the Ohio Range, the range of WAIS surface lowering is more variable, with down draw of up to 600 m occurring during full collapse events.

Similar to observations in the Ohio Range prominent peaks in the exposure age distribution (Fig. 8c) occur during periods of rapidly rising ice elevation (10–20 ka and 80 to 90 ka). The pronounced peak between 40 and 50 ka corresponds with the end of an interval of relatively high ice elevations and temperature. In contrast to the simulated elevation history in the Ohio Range, average simulated WAIS elevations near Mt. Waesche are lower than present. In the model elevation history, down draw of the ice surface associated with collapse of the marine portions of the WAIS is ~200 m, again occurring after isotope stage 5c rather than at 5e. If full collapse had been triggered during stage 5e in the model simulation, lowering of the WAIS surface would begin earlier and down draw increased to as much as 600 m based on other down-draw events earlier in the simulation (Fig. 6). Thus, assuming a full collapse event occurred during stage 5e, the model simulation indicates that the ice elevations would not recover to near present elevations until between 80 ka and 90 ka (dashed line Fig. 8b). In either case, the relative highstand at ~85 ka corresponds to the largest peak in the PDF from Mt. Waesche.

Assuming the simulated elevation history for Mt. Waesche is generally correct, we evaluate models for the deposition and exposure histories of moraine boulders at Mt. Waesche (Section 2.3). For example, one model assumes that simple exposure (no prior exposure or cover) of the boulders occurs after deposition on the flank of Mt. Waesche. However, if the actual ice sheet elevations were lower than present between 20 ka and 100 ka as simulated by the ice sheet model, boulders could not have been deposited on the flanks of Mt. Waesche above the present ice elevation during that time interval. Thus, boulders with exposure ages between 40 ka and 90 ka would not occur on the slopes of Mt. Waesche above the present ice surface. Similarly, if the simulated elevation history is

Author's personal copy

correct, boulders could not have been deposited prior to ~100 ka and subsequently been ice-covered for long periods resulting in apparent exposure ages between 40 ka and 90 ka because in the simulation, ice elevations above present occur only rarely following terminations (Fig. 6). Thus, no simple exposure history, nor one involving periods of cover, would result in apparent exposure ages between 40 ka and 90 ka consistent with the simulated elevation history. In contrast, models involving long prior exposure on the blue ice, no cover (Ackert et al., 2011; Fogwill et al., 2012) and short subsequent exposure on the flank of Mt. Waesche are consistent with the simulated elevation history.

The dearth of exposure ages older than 100 ka at Mt. Waesche is consistent with clearance of older debris from the blue ice area during draw down of the WAIS surface during the Last Interglacial as indicated in the simulated elevation history, particularly if down draw was as much as 600 m (Fig. 8b). Deposition of glacial debris during the draw down could have occurred on the slopes of the volcano below the present ice surface, or alternatively debris may have been swept away under a different ice flow regime. The oldest dated tephra layer (117 ± 7 ka) within the blue ice at Mt. Waesche is consistent with the ice around Mt. Waesche having formed since the Last Interglacial (Dunbar et al., 2007). We hypothesize that bands of supra-glacial debris began accumulating on the blue ice after ice elevations had recovered to near the present-day level at ~90 ka (Fig. 8b). In contrast to the present situation where the supra-glacial debris has little exposure, the debris remained on the blue ice surface accumulating exposure. Potentially analogous accumulations of debris are extensive areas of ice-cored moraine on the WAIS surface at Mt. Sidley 20 km south east of Mt. Waesche. During the last highstand at ~12 ka, basalt clasts with prior exposure ranging up to ~80 ka were deposited on the flank of the volcano, forming the upper moraine band. The lower moraine band with its tight cluster of exposure ages likely represents the emergence of a large pulse of englacial debris at ~10 ka.

In the model simulation, the penultimate highstand at Mt. Waesche occurs during the Last Interglacial (stage 5e) at an elevation ~20 m higher than the most recent highstand, suggesting that the upper moraine band (+80 m) may have been deposited during the Last Interglacial and that only the lower moraine band (+45 m) was deposited during the last highstand. In fact, one exposure age dates to the penultimate highstand consistent with this interpretation. However, an exposure age of ~12 ka occurs at the same location and an exposure age of ~17 ka occurs 10 m below (Table 2). Thus, it is possible that the WAIS may have reached the elevation of the upper moraine band during the last two highstands. Alternatively, the boulders with younger ages may have been exhumed by cryoturbation or be the remains of larger, recently fractured boulders. However, given the non random exposure age distribution, we find the latter possibility unlikely. Thus, deposition of part of the upper moraine band, during either the last or penultimate highstand, is consistent with the simulated elevation history.

Overall, the timing and magnitude of WAIS highstands at Mt. Waesche and the Ohio Range Escarpment is similar and is captured by the continental ice sheet model. The distribution of exposure ages at Mt. Waesche and the Ohio Range over the past 100 ka is also similar and likely reflects common processes. Therefore, we infer that the peaks in exposure age distributions at the two sites are associated with pulses of debris that emerge out of the ice and accumulate in local ablation areas during intervals of relatively stable or rising ice elevations. Supra-glacial debris with a range of prior exposure was then deposited on Mt. Waesche and the Ohio Range Escarpment during WAIS highstands and subsequent down draw of the WAIS.

5. Conclusions

The exposure ages of glacial boulders at both Mt. Waesche and the Ohio Range on opposite ends of the WAIS divide, primarily record the integrated duration of exposure at the site where the samples were collected and/or exposure on adjacent topographically-controlled blue ice areas. Similar distributions of exposure ages of erratics with peaks around 10 ka, 40 ka and 80 ka on the Ohio Range Escarpment, nearby Mercer Ridge on Mt. Schopf, and Mt. Waesche in Marie Byrd Land, suggests the WAIS and alpine glaciers were responding to a common forcing at all three sites. Maximum WAIS elevations were reached between 10 ka and 12 ka in both Marie Byrd Land and the Ohio Range. We infer that the peaks in the exposure age distributions record pulses of englacial debris emergence in the ablation zone associated with warmer temperatures.

The good correspondence between the simulated WAIS elevation history and the geologic constraints on the timing and height of the last highstand at two widely separated sites in interior West Antarctica suggests that the ice sheet model accurately simulates interior WAIS dynamics. The observed peaks in the exposure age distributions correspond to increasing ice elevation leading to, and including, the highstands. The ice sheet model indicates that interior WAIS elevation was generally higher than present at the Ohio Range, but lower than present at Mt. Waesche. Simulated down-draw of the WAIS surface during the Last Interglacial was ~200 m at the Ohio Range and possibly as much as 600 m at Mt. Waesche. The occurrence of maximum interior WAIS elevations following glacial terminations appears to be a robust feature of the ice sheet model and is consistent with the geologic evidence from the last highstand at both the Ohio Range and Mt. Waesche.

The success of the ice sheet model in capturing temperature-driven elevation changes in interior West Antarctica is surprising, given the simple parameterization of ocean-melt variations scaled mainly to marine $\delta^{18}O$ (essentially a Northern Hemispheric climate signal) plus a minor contribution of austral summer insolation intensity. The general correspondence of the model results and geologic evidence suggests that the use of marine $\delta^{18}O$ as the major forcing factor is justified as a first step. The dominance of marine $\delta^{18}O$ in our forcing probably reflects the fact that temperature anomalies in interior Antarctica occur on a background of global CO_2-driven temperature variation, which co-varies closely with $\delta^{18}O$ (Petit et al., 1999). As a result, the warmest temperatures, highest accumulation rates and hence, highest interior WAIS elevations occur after the glacial terminations, prior to down draw or collapse driven by the retreating grounding line.

Acknowledgments

The authors acknowledge logistical support from Raytheon Polar Services, Air National Guard, and Kenn Borek Air. We specially acknowledge the help and support from Peter Braddock during fieldwork in the Ohio Range. The authors also acknowledge John Stone for the use of his cosmogenic isotope laboratory and Brad Singer for making the argon isotope measurements. AP thanks the Gary Comer Science and Education Foundation for support. This project was funded by OPP-0087709 to MK and RA and OPP grant 0338271 to SM and 0338189 to HB.

Appendix A. Supplementary data

Supplementary data related to this article can be found at http://dx.doi.org/10.1016/j.quascirev.2012.12.017.

Author's personal copy

References

Ackert Jr., R.P., Barclay, D.J., Borns Jr., H.W., Calkin, P.E., Kurz, M.D., Steig, E.J., Fastook, J.L., 1999. Measurement of ice sheet elevations in interior West Antarctica. Science 286, 276–280.

Ackert Jr., R.P., 2000. Antarctic Glacial Chronology: New Constraints from Surface Exposure Dating. Ph.D. thesis, MIT/WHOI Joint Program in Oceanography.

Ackert Jr., R.P., Kurz, M.D., 2004. Age and uplift rates of Sirius Group sediments in the Dominion Range Antarctica, from surface exposure dating and geomorphology. Glob. Planet. Change 42, 207–225.

Ackert Jr., R.P., Mukhopadhyay, S., Parizek, B.R., Borns, H.W., 2007. Ice elevation near the West Antarctic Ice Sheet divide during the Last Glaciation. Geophys. Res. Lett. 34, L21506. http://dx.doi.org/10.1029/2007GL031412.

Ackert Jr., R.P., Mukhopadhyay, S., Pollard, D., DeConto, R.M., Putnam, A.E., Borns, H.W., 2011. West Antarctic Ice Sheet elevations in the Ohio Range: geologic constraints and ice sheet modeling prior to the last highstand. Earth Planet. Sci. Lett. 307, 83–93. http://dx.doi.org/10.1016/j.epsl2011.04.015.

Alley, R.B., Whillans, I.M., 1984. Response of the East Antarctica ice sheet to sea-level rise. J. Geophys. Res. 89, 6487–6493.

Anderson, J.B., Shipp, S.S., Lowe, A.L., Wellner, J.S.,, Mososla, A.B., 2002. The Antarctic ice sheet during the last glacial maximum and its subsequent retreat history; a review. Quat. Sci. Rev. 21, 49–70.

Balco, G., Shuster, D.L., 2009. Production rate of ^{21}Ne in quartz estimated from ^{10}Be, ^{26}Al and ^{21}Ne concentrations in slowly eroding Antarctic bedrock surfaces. Earth Planet. Sci. Lett. 281, 48–58.

Bamber, J.L., Riva, R.E.M., Vermeersen, B.L.A., LeBrocq, A.M., 2009. Reassessment of the potential sea-level rise from a collapse of the west Antarctic Ice Sheet. Science 324, 901–903. http://dx.doi.org/10.1126/Science.1169338.

Bentley, M.J., Fogwell, C.J., LeBrocq, A.M., Hubbard, A.L., Sugden, D.E., Dunai, T., Freeman, S.P.H.T., 2010. Deglacial history of the West Antarctic Ice Sheet in the Weddell Sea embayment: constraints on past ice volume change. Geology 38, 411–414. http://dx.doi.org/10.1130/G30754.1.

Brook, E.J., Kurz, M.D., 1993. Surface-exposure chronology using *in situ* cosmogenic ^{3}He in Antarctic quartz sandstone boulders. Quat. Res. 39, 1–10.

Dunbar, N.W., McIntosh, W.C., Kurbatov, A.V., Wilch, T.I., 2007. Integrated Tephrochronology of the West Antarctic Region: Implications for a Potential Tephra Record in the West Antarctic Ice Sheet (WAIS) Divide Ice Core, Open-File Report, USGS OF-2007-1047, Extended Abstract 179. U.S Geological Survey, 4.

Fogwill, C.J., Hein, A.S., Bentley, M.J., Sugden, D.E., 2012. Do blue-ice moraines in the Heritage Range show that the West Antarctic Ice Sheet survived the last interglacial? Palaeogeo. Palaeoclim. Palaeoeco. 335–336, 61–70. http://dx.doi.org/10.1016/j.palaeo.2011.01.027.

Gayer, E., Mukhopadhyay, S., Meade, B.J., 2008. Spatial variability of erosion rates inferred from the frequency distribution of cosmogenic ^{3}He in olivines from Hawaiian river sediments. Earth Planet. Sci. Lett. 266, 303–315. http://dx.doi.org/10.1016/j.epsl.2007.11.019.

Goehring, B.M., Kurz, M.D., Balco, G., Schaefer, J.M., Licciardi, J., Lifton, N., 2010. A reevaluation of in situ cosmogenic ^{3}He production rates. Quat. Geochron. 5, 410–418.

Huybers, P., Denton, G.H., 2008. Antarctic temperature at orbital timescales controlled by summer duration. Nat. Geosci. 1, 787–792. http://dx.doi.org/10/1038/ngeo311.

Ivy-Ochs, S., Schlüchter, C., Kubik, P.W., Dittrich-Hannen, B., Beer, J., 1995. Minimum ^{10}Be exposure ages of early Pliocene for the Table Mountain plateau and the Sirius Group at Mount Fleming, Dry Valleys, Antarctica. Geology 23, 1007–1010.

Johnsen, S.J., Dansgaard, W., Clausen, H.B., Langway, C.C.J., 1972. Oxygen isotope profiles through the Antarctic and Greenland ice sheets. Nature 235, 429–434.

Johnson, J.S., Bentley, M.J., Gohl, K., 2008. First exposure ages from the Amundsen Sea Embayment, West Antarctica: the Late Quaternary context for recent thinning of Pine Island, Smith and Pope glaciers. Geology 36, 223–226. http://dx.doi.org/10.1130/G24207A.1.

Kaplan, M.R., Strelin, J.A., Schaefer, J.M., Denton, G.H., Finkel, R., Schwartz, R., Putnam, A.E., Vandergoes, M.J., Goehing, B.M., Travis, S.G., 2011. In-situ cosmogenic ^{10}Be production rate at Lago Argention, Patagonia: implications for late glacial chronology. Earth Planet. Sci. Lett. 309, 21–32. http://dx.doi.org/10.1016/j.epsl.2011.06.018.

Kawamura, K., Parrenin, F., Lisiecki, L., Uemura, R., Vimeux, F., Severinghaus, J.P., Hutterli, M.A., Nakazawa, T., Aoki, S., Jouzel, J., Raymo, M.E., Matsumoto, K., Nakata, H., Motoyama, H., Fujita, S., Goto-Azuma, K., Fujii, Y., Watanabe, O., 2007. Northern Hemisphere forcing of climatic cycles in Antarctica over the past 360,000 years. Nature 488, 912–916.

Kurz, M.D., 1986. Cosmogenic helium in a terrestrial igneous rock. Nature 320, 435–439.

Kurz, M.D., Kenna, T.C., Lassiter, J.C., DePaolo, D.J., 1996. Helium isotopic evolution of Mauna Kea Volcano: first results from the 1-km drill core. J. Geophys. Res. 101, 11,781–711,791.

LeMasurier, W., Kawachi, Y., 1990. Mt. Waesche. In: LeMasurier, W., Thompson, J.W. (Eds.), Volcanoes of the Antarctic Plate and Southern Oceans, vol. 48. American Geophysical Union, Washington D. C., pp. 208–211.

LeMasurier, W., Rex, D.C., 1989. Evolution of linear volcanic ranges in Marie Byrd Land, West Antarctica. J. Geophys. Res. 94, 7223–7236.

Len Vacher, H., Hearty, P., 1989. History of stage 5 sea level in Bermuda: review with new evidence of a brief rise to present sea level during Substage 5a. Quat. Sci. Rev. 82, 159–168.

Lilly, K., Fink, D., Fabel, D., Lambeck, K., 2010. Pliocene dynamics of the interior East Antarctic Ice sheet. Geology 38, 703–706. http://dx.doi.org/10.1130/G31172x.1.

Liu, B., Phillips, F.M., Fabryka-Martin, J.T., Fowler, M.M., Stone, W.D., 1994. Cosmogenic ^{36}Cl accumulation in unstable landforms1. Effects of the thermal neutron distribution. Water Resour. Res. 30, 3115–3125.

Mackintosh, A., White, D., Fink, D., Gore, D.B., Pickard, J., Fanning, P.C., 2007. Exposure ages from mountain dipsticks in Mac. Robertson Land, East Antarctica, indicate little change in ice thickness since the Last Glacial Maximum. Geology 35, 551–554. http://dx.doi.org/10.1130/G23503A.1.

Masarik, J., Reedy, R.C., 1996. Monte Carlo simulation of the in-situ-produced cosmogenic nuclides. Radiocarbon 38, 163.

Mercer, J.H., 1963. Glacial Geology of the Ohio Range, Central Horlick Mountains, Antarctica. Institute of Polar Studies, 8,. Ohio State University Research Foundation. 13 p.

Mercer, J.H., 1978. West Antarctic ice sheet and the CO_2 greenhouse effect: a threat of disaster. Nature 271, 321.

Mukhopadhyay, S., Ackert, J.,R.P., Pope, A.E., Pollard, D., DeConto, R.M., 2012. Miocene to recent ice elevation variations from the interior of the West Antarctic ice sheet: constraints from geologic observations, cosmogenic nuclides and ice sheet modeling. Earth Planet. Sci. Lett. 337–338, 243–251. http://dx.doi.org/10.1016/j.epsl.2012.05.015.

Nishiizumi, K., Kohl, C.P., Arnold, J.R., Klein, J., Fink, D., 1991. Cosmic ray produced ^{10}Be and ^{26}Al in Antarctic rocks: exposure and erosion rates. Earth Planet. Sci. Lett. 104, 440–454.

Pollard, D., DeConto, R.M., 2009. Modelling West Antarctic ice sheet growth and collapse through the past five million years. Nature 458, 329–333. http://dx.doi.org/10.1038/nature07809.

Pollard, D., DeConto, R.M., 2012a. Description of a hybrid ice sheet-shelf model, and application to Antarctica. Geosci. Model. Devel. Discussion 5, 1077–1134.

Pollard, D., DeConto, R.M., 2012b. A simple inverse method for the distribution of basal sliding coefficients under ice sheets, applied to Antarctica. Cryoshere Discuss. 6, 1405–1444.

Petit, J.R., Jouzel, J., Raynaud, D., Barkov, N.I., Barnola, J.-M., Basile, I., Bender, M., Chappellaz, J., Davis, M., Delaygue, G., Delmotte, M., Kotlyakov, V.M., Legrand, M., Lipenkov, V.Y., Lorius, C., Pepin, L., Ritz, C., Saltzman, E., Stievenard, M., 1999. Climate and atmospheric history of the past 420,000 years from the Vostock ice core, Antarctica. Nature 399, 429–436.

Price, S.F., Conway, H., Waddington, E.D., 2007. Evidence for late Pleistocene thinning of Siple Dome. J. Geophys. Res. 112, F03021.

Putnam, A.E., Schaefer, J.M., Barrell, D.J.A., Vandergoes, M.D., Denton, G.H., Kaplan, M.R., Finkel, R.C., Schwartz, R., Goehring, B.M., Kelley, S.E., 2010. In situ cosmogenic Be-10 production-rate calibration from the Southern Alps, New Zealand. Quat. Geochron. 5, 392–409.

Singer, B.S., Ackert Jr., R.P., Guillou, H., 2004. ^{40}Ar/^{39}Ar and K–Ar chronology of Pleistocene glaciation in Patagonia. Geologicial Soc. America Bull. 116, 434–450.

Steig, E.J., Fastook, J.L., Zweck, C., Goodwin, I., Licht, K.L., White, J.W.C., Ackert Jr., R.P., 2001. West Antarctic Ice Sheet elevation changes. In: Alley, R.B., Bindschadler, R.A. (Eds.), The West Antarctic Ice Sheet; Behavior and Environment. Antarctic Research Series, vol. 77. American Geophysical Union, pp. 75–90.

Stone, J.O., Allan, G.L., Fifield, K.L., Cresswell, R.G., 1996a. Cosmogenic chorine-36 from calcium spallation. Geochim. Cosmchim. Acta 60, 679–692.

Stone, J.O., Evans, J.M., Fifield, K.L., Cresswell, R.G., Allan, G.L., 1996b. Cosmogenic chorine-36 production rates from calcium and potassium. Radiocarbon 38, 170–171.

Stone, J.O., Evans, J.M., Fifield, K.L., Allan, G.L., Cresswell, R.G., 1998. Cosmogenic chorine-36 production in calcite by muons. Geochim. Cosmchim. Acta 62, 433–454.

Stone, J.O., 2000. Air pressure and cosmogenic isotope production. J. Geophys. Res. 105 (B10), 23,753–23,759.

Stone, J.O., Balco, G.A., Sugden, D.E., Caffee, M.W., Sass I., L.S., Cowdrey, S.G., Siddoway, C., 2003. Holocene deglaciation of Marie Byrd Land, West Antarctica. Science 299, 99–102.

Todd, C., Stone, J., Conway, H., Hall, B.R., Bromley, G., 2010. Late Quaternary evolution of Reedy Glacier, Antarctica. Quat. Sci. Rev. 29, 1328–1341. http://dx.doi.org/10.1016/j.quascirev.2010.02.001.

Waddington, E.D., Conway, H., Steig, E.J., Alley, R.B., Brook, E.J., Taylor, K.C., White, J.W.C., 2005. Decoding the dipstick: thickness of Siple Dome, West Antarctica, at the Last Glacial Maximum. Geology 33, 281–284.